

Spatial Graph Convolutions for Drug Discovery

Evan N. Feinberg,¹ Debnil Sur,² Brooke E. Husic,³ Doris Mai,² Yang Li,⁴ Jianyi Yang,⁴ Bharath Ramsundar,² and Vijay S. Pande^{5, a)}

¹⁾*Program in Biophysics, Stanford University*

²⁾*Department of Computer Science, Stanford University*

³⁾*Department of Chemistry, Stanford University*

⁴⁾*School of Mathematical Sciences and College of Life Sciences, Nankai University*

⁵⁾*Department of Bioengineering, Stanford University*

ABSTRACT

Predicting the binding free energy, or affinity, of a small molecule for a protein target is frequently the first step along the arc of drug discovery. High throughput experimental and virtual screening both suffer from low accuracy, whereas more accurate approaches in both domains suffer from lack of scale due to either financial or temporal constraints. While machine learning (ML) has made immense progress in the fields of computer vision and natural language processing, it has yet to offer comparable improvements over domain-expertise driven algorithms in the molecular sciences. In this paper, we propose new Deep Neural Network (DNN) architectures for affinity prediction. The new model architectures are at least competitive with, and in many cases state-of-the-art compared to previous knowledge-based and physics-based approaches. In addition to more standard evaluation metrics, we also propose the Regression Enrichment Factor $EF_{\chi}^{(R)}$ for the community to benchmark against in future affinity prediction studies. Finally, we suggest the adaptation of an agglomerative clustering cross-validation strategy to more accurately reflect the generalization capacity of ML-based affinity models in future works.

I. INTRODUCTION

Most FDA-approved drugs are small organic molecules that elicit a therapeutic response by binding to one or more biological macromolecules. Once bound to the macromolecular target, small molecule ligands achieve their function by competitively inhibiting the binding of an endogenous ligand or by allosterically adjusting the conformational ensemble of that macromolecule. Regardless of specific mode of action, binding is a necessary if not always sufficient behavior of a therapeutic ligand. To maximize the therapeutic index – roughly, the ratio of desired therapeutic effect to toxicity – of a molecule, it is necessary to at once maximize the affinity, or binding free energy (ΔG), of that molecule for the desired targets while minimizing its affinity for other macromolecules.

Historically, scientists have taken both cheminformatic and structure-based approaches to model ligands and the

macromolecules to which they bind. While initially developed for the domain of computer vision, artificial neural networks, or deep neural networks (DNNs), have recently been translated to the molecular sciences. Virtually all preceding machine learning (ML) approaches are predicated on either domain expertise-driven features or rigid formulations of simpler features. In contrast, the central attraction of DNNs is arguably its ability to hierarchically and differentially learn more complex featurizations best suited to the specific task of interest. Fully connected neural networks entail series of matrix multiplications and pointwise nonlinearities that iteratively combine features inputted as fixed length vectors. However, the most successful DNN architectures are constructed to exploit the unique structure of the data at hand. For instance, convolutional neural networks (CNNs) leverage the information encoded in proximity between pixels in images, whereas recurrent neural networks balance the significance of both neighboring and separated blocks of text in modeling natural language.

In approaching the problem of protein-ligand binding affinity prediction, one might be tempted to draw an analogy to computer vision problems. Just as neighboring pixels connote closeness between physical objects, one could subdivide a binding pocket into a grid of voxels, where neighboring voxels denote neighboring atoms and blocks of empty space. Unfortunately, such a 3D CNN approach has several potential drawbacks. First, it is highly memory intensive in both the inputs and in the hidden weights. Second, the parameters, growing exponentially as the number of dimensions, suffer from a “curse of dimensionality”^{1,2}; whereas a 3×3 filter for image processing contains 9 parameters, a $3 \times 3 \times 3$ filter for molecule processing contains 27 parameters.

In contrast, graph convolutions limit the number of parameters by exploiting the structure and symmetry inherent in molecules. By treating atoms as nodes and bonds as edges, graph convolutions can be viewed as a hierarchical, differentiable, and flexible analogy to the commonly used circular fingerprint representation in cheminformatics. To represent a carbon bonded to four other atoms, for example, a 3D CNN will need several different filters to accommodate the many symmetrically equivalent orientations that such a functional subgroup can undertake. In contrast, a graph convolution as described in 3–6 is symmetric to permutations and relative location of each of the four neighboring atoms, thereby saving a sizable number of parameters. Since reducing number of parame-

^{a)}Electronic mail: pande@stanford.edu

ters generally leads to a lower variance model, the graph convolution is attractive for molecules in the same way that 2D CNNs are attractive for images.

In this paper, we first review a subset of DNN architectures applicable to protein-ligand interaction. By introducing the mathematical frameworks previously investigated, we provide context to motivate the new models we present and test in the latter portion of the paper. These new models generalize the concept of a graph convolution to include noncovalent interactions between different molecules in addition to intramolecular interactions. First, we describe a staged gated graph neural network which distinguishes the derivation of differentiable bonded atom types from the propagation of information between different molecules. Second, we describe a more flexible model based on a new update rule predicated on both the distance of a source atom to a target atom as well as on the feature map of the target atom. Unlike 6, which focuses on ligand-only quantum mechanics tasks, in this work we notice that incorporating information on target atoms directly in the message function leads to increased signal in certain protein-ligand binding affinity benchmarks. Finally, we address a potential shortcoming of the standard benchmark in this space—treating the PDBBind 2007 core set as a fixed test set—by suggesting a new cross-validation strategy for this canonical dataset. By generating a test set drawn from a different distribution than the train or validation sets, we propose that, in the future, the community measure affinity prediction methods with this more challenging benchmark that may better reflect the generalization capacity of a given model.

II. NEURAL NETWORK ARCHITECTURES

First, we briefly review a subset of DNN architectures applicable to protein-ligand interaction in order to motivate the new models we present and test at the end of the paper.

A. Ligand-based scoring models

1. Fully Connected Neural Networks

The perhaps qualitatively simplest models for affinity prediction incorporate only features of ligands and ignore any information about the macromolecular target(s) of interest. A model built on such features might entail a fully connected neural network (FCNN). In a FCNN, each molecule is represented by a flat vector $[x_0, \dots, x_{f_0}] = x$ containing f_0 features. Then, these features are sequentially transformed into so-called "hidden" representations by applying a nonlinear activation layer to the product of a weight matrix W and the current representation (this process is often called an "update"). Algebraically, for K hidden layers, we have,

$$\begin{aligned} h^{(1)} &= \text{ReLU} \left(W^{(1)} \cdot x \right) \\ h^{(2)} &= \text{ReLU} \left(W^{(2)} \cdot h^{(1)} \right) \\ &\vdots \\ h^{(K)} &= W^{(K)} \cdot h^{(K-1)}, \end{aligned} \tag{1}$$

wherein the final hidden layer, $h^{(K)}$, would be a 1×1 scalar output and $W^{(K)} \in \mathbb{R}^{(1 \times f_{K-1})}$. The rectified linear unit (*ReLU*) is an example activation function that returns the maximum of the input and 0⁷, but could be replaced with other nonlinear functions.

The training data for such a network consists of a set of N molecules, each represented by a flat vector of length f_0 , which have a one-to-one correspondence to a set of N affinity labels. In practice, one might generate such features using one or more of a variety of cheminformatic software packages, such as RDKit⁸, OEChem⁹, OpenBabel¹⁰, or DeepChem¹¹. Domain-expertise driven flat vector features might include integer counts of different types of pre-determined functional groups (e.g., carboxylic acids, aromatic rings), polar atoms, nonpolar atoms, estimated values of pKa, solvation free energy, and other ligand-based features. Alternatively, the cheminformatic community has proposed featurizations that may be viewed as a compromise between the hand-crafted featurizations of older statistical learning methods and the more elementary featurizations meant to exploit the structure of data found in deep learning approaches. Such cheminformatic featurizations include Extended Circular Fingerprints (ECFP), otherwise known as Morgan Fingerprints¹², which amount to hashing local neighborhoods within ligands into a vector with a fixed number of bits. Other cheminformatic methods like ROCS¹³ can be decomposed into its functional components for use in featurization¹⁴.

2. Graph Convolutional Neural Networks

Convolutional neural networks (CNNs) are a common framework utilized for image analysis often on 2D grids of pixels¹⁵. Each layer of a CNN convolves the previous layer’s feature map with linear kernels followed by elementwise nonlinearities, producing new features of higher complexity that combine information from neighboring pixels.

A graph convolutional neural network (GCNN) exploits the inherent structure of data that is organized into a network analogously to how traditional convolutional neural networks exploit the spatial adjacency of a grid of Euclidean data¹⁶. A graph is a data structure consisting of a series of nodes, features describing those nodes, and edges that denote connections between those nodes (and, in some networks, features for each edge). If there are N nodes in a given graph, f_{in} features per node, and a

single edge type, we can represent this graph as consisting of node features x and symmetric adjacency matrix A , which designates whether a pair of nodes belong to each other’s neighbor sets N :

$$x = \begin{bmatrix} x_{11} & x_{12} & \cdots & x_{1f_{in}} \\ x_{21} & x_{22} & \cdots & x_{2f_{in}} \\ \vdots & \vdots & \ddots & \vdots \\ x_{N1} & x_{N2} & \cdots & x_{Nf_{in}} \end{bmatrix} \in \mathbb{R}^{N \times f_{in}} \quad (2)$$

$$A = \begin{bmatrix} 0 & A_{12} & \cdots & A_{1N} \\ A_{21} & 0 & \cdots & A_{2N} \\ \vdots & \vdots & \ddots & \vdots \\ A_{N1} & A_{N2} & \cdots & 0 \end{bmatrix} \in \mathbb{R}^{N \times N}, \quad (3)$$

$$\text{where: } A_{ij} = \begin{cases} 1, v_j \in N(v_i) \\ 0, \text{otherwise.} \end{cases}$$

While this mathematical framework is general and crisp, it is also instructive to examine its application to a specific example. Suppose one is analyzing properties of the molecule propanamide, an amide with a three-carbon chain (Figure 1). Labeling the carbons from left to right as (1), (2), and (3), the oxygen as (4), and the nitrogen as (5), and using very simple features, where columns 1-3 of x denote one-hot vectors of elements and columns 4-5 are one-hot vectors of hybridization type, we can write the following matrices:

$$x = \begin{bmatrix} 1 & 0 & 0 & 0 & 1 \\ 1 & 0 & 0 & 0 & 1 \\ 1 & 0 & 0 & 1 & 0 \\ 0 & 1 & 0 & 1 & 0 \\ 0 & 0 & 1 & 0 & 1 \end{bmatrix}, A = \begin{bmatrix} 0 & 1 & 0 & 0 & 0 \\ 1 & 0 & 1 & 0 & 0 \\ 0 & 1 & 0 & 1 & 1 \\ 0 & 0 & 1 & 0 & 0 \\ 0 & 0 & 1 & 0 & 0 \end{bmatrix}. \quad (4)$$

A graph convolution update entails applying a function at each node that takes as input both that node and its neighbors and outputs a new set of features for each of the N nodes. A spate of graph convolutional architectures have been proposed, and well summarized in 6, span the common framework,

$$h_i^{(t+1)} = U^{(t)} \left(h_i^{(t)}, \sum_{v_j \in N(v_i)} m^{(t)}(h_j^{(t)}) \right), \quad (5)$$

where $h_i^{(t)}$ represents the node features of node i at hidden layer t , $N(v_i)$ represents the neighbors of node i , and $U^{(t)}$ and $m^{(t)}$ are the update and message functions, respectively, at hidden layer t . An important nuance is the possibility of multiple edge types. In this case, we must define multiple message functions, $m^{(t,e)}$, which is the message function at layer t for edge type $e \in [1, \dots, N_{et}]$.

By analogy to FCNNs (1, reproduced left), we can write the qualitatively simplest possible graph convolutional neural network can be written as follows (right),

$$\begin{aligned} h^{(1)} &= \text{ReLU} \left(W^{(1)} \cdot x \right) & h^{(1)} &= \text{ReLU} \left(W^{(1)} A \cdot x \right) \\ h^{(2)} &= \text{ReLU} \left(W^{(2)} \cdot h^{(1)} \right) & h^{(2)} &= \text{ReLU} \left(W^{(2)} A \cdot h^{(1)} \right) \\ &\vdots & &\vdots \\ h^{(K)} &= W^{(K)} \cdot h^{(K-1)} & h^{(K)} &= \text{ReLU} \left(W^{(K)} A \cdot h^{(K-1)} \right). \end{aligned} \quad (6)$$

We see that the most apparent difference between update (1) and (6) is the additional factor of the $N \times N$ adjacency matrix A , which remains constant at each layer of the update. The A factor enables information to propagate further in the network at each layer. For practitioners, we should note that, if one is to use the GCNN in (6), one would need to add ones to the adjacency matrix in (3) and (4) along the diagonal.

In this paper, our models are primarily inspired by one of the more complex realizations of (5): the Gated Graph Neural Networks (GGNNs)⁵. In the GGNN framework, update functions are defined as the gated recurrent unit (GRU), a recurrent neural network operation (which is

the same function at all layers), while message functions are simple linear operations that are different for each edge type but, like the update function, also remain the same across layers,

$$h_i^{(t+1)} = \text{GRU} \left(h_i^{(t)}, \sum_e^{N_{et}} W^{(e)} A^{(e)} h^{(t)} \right), \quad (7)$$

where $A^{(e)}$ is the adjacency matrix, and $W^{(e)}$ the weight matrix, respectively, for edge type e . For example, using the notation introduced above, we can write a K-layer GCNN update as,

$$\begin{aligned}
 h^{(1)} &= GRU \left(x, \sum_e^{N_{et}} W^{(e)} A^{(e)} x \right) \\
 h^{(2)} &= GRU \left(h^{(1)}, \sum_e^{N_{et}} W^{(e)} A^{(e)} h^{(1)} \right) \\
 &\vdots \\
 h^{(K)} &= GRU \left(h^{(K-1)}, \sum_e^{N_{et}} W^{(e)} A^{(e)} h^{(K-1)} \right),
 \end{aligned} \tag{8}$$

where $W(e)$ is the $f_{in} \times f_{in}$ weight matrix for edge type e and $h^{(t)}$ are the $N \times f_{in}$ node embeddings at layer t .

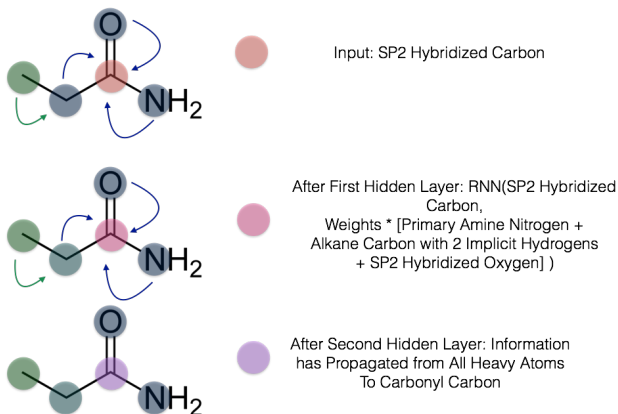


FIG. 1. Visual depiction of Gated Graph Neural Network with atoms as nodes and bonds as edges. The small molecule propanamide is chosen to illustrate the propagation of information among the different update layers of the network.

In contrast to update (1), which learns non-linear combinations of the input hand-crafted features, the update described in (8) learns complex information about molecules from even more basic features. At each layer, new per-atom feature maps are derived from a nonlinear combination of the features of a given atom with the features of its immediate neighbors. Therefore, for a given query atom i , successive applications of a graph convolution mean that information propagates from other atoms $\{j\}$ successively further away by measure of minimum bond-path length.

For example, while ECFP-2, ECFP-4, and ECFP-6 confer information on atomic neighborhoods of increasing radius with a fixed, non-differentiable form, successive layers of graph convolutions pass information with atomic neighborhoods of increasing radius in a flexible way that can learn non-integer atom types. The GRU update function confers an additional contrast to circular fingerprints. Whereas ECFP- n incorporates all information from the up-to $\sum_{i=1}^{\frac{n}{2}} 4^{i-1}$ atoms in the hashed neighborhood, the GRU update in (8) adds information *selectively* from further atoms to the current atom; with its combined “update” and “forget” gates, it allows more complex feature maps to be learned with greater efficiency.

Whereas (1) is predicated on graph-level hand-crafted features only, (8) contains both basic per-node features in $x \in \mathbb{R}^{N \times f_{in}}$ as well as structural information in $A \in \mathbb{R}^{N \times N}$. State of the art ligand-based models^{6,11} begin with such simple one-hot data as the element, hybridization type, number of implicit hydrogens, valence of the atom, and aromaticity of the atom represented by each node. Referring again by example to the propanamide example from equation 4, traditional featurizations like ECFP-4 would entail a single feature vector $x \in \mathbb{R}^{1 \times f_{in}}$ with counts of each type of functional group whose indices are derived by hashing a string representation of that functional group. FCNN’s based on an ECFP-4-derived x at each layer would involve non-linear combinations of counts of these hashed functional groups.

By contrast, represented as a graph, input features x for propanamide would consist of the simple atom-level features described in Table IV. Focusing again as a case study on the carbonyl carbon, the first layer of a GCNN would lead that carbonyl carbon, originally represented by $x_i \in \mathbb{R}^{1 \times f_{in}}$ to have new features $h_i \in \mathbb{R}^{1 \times f_1}$ that is a nonlinear function of the carbonyl carbon’s features x_i and that of its neighboring oxygen, nitrogen, and carbon features $\{x_j\}$. One further GCNN update would propagate signal from the terminal alkyl carbon of propanamide to the carbonyl carbon (Figure 1).

In both classification and regression settings, GCNN’s terminate in a “graph gather” step, which is invariant to node ordering, followed by FCNNs to produce output of the desired size (f_{out}). In this work, we generally use the graph gather update shown in (9), which is as a sum over the rows r of the final node embeddings $h^{(f)} = \sigma(i(h^{(K)}, x)) \odot (j(h^{(K)}))$, where i and j are single layer FCNNs. This completes the standard graph convolutional update used in this paper,

$$\begin{aligned}
h^{(1)} &= GRU \left(x, \sum_e^{N_{et}} W^{(e)} A^{(e)} x \right) \\
h^{(2)} &= GRU \left(h^{(1)}, \sum_e^{N_{et}} W^{(e)} A^{(e)} h^{(1)} \right) \\
&\vdots \\
h^{(K)} &= GRU \left(h^{(K-1)}, \sum_e^{N_{et}} W^{(e)} A^{(e)} h^{(K-1)} \right) \\
h^{(FC_0)} &= \sum_{r=1}^N \left[\sigma \left(i(h^{(K)}, x) \right) \odot \left(j(h^{(K)}) \right) \right]_r \\
&\in \mathbb{R}^{(1 \times f_{out})} \\
h^{(FC_1)} &= ReLU \left(W^{(FC_1)} \cdot h^{(FC_0)} \right) \\
&\vdots \\
h^{(FC_M)} &= ReLU \left(W^{(FC_M)} \cdot h^{(FC_{M-1})} \right).
\end{aligned} \tag{9}$$

3. Generalization to multitask settings

In the context of affinity prediction, one would typically train GCNN’s as described in (9) on an affinity dataset for either a single target or multiple targets. The latter set-

ting can be implemented by either training different models for each target or by training a single multitask network wherein the last weight matrix $W^{(FC_M)} \in \mathbb{R}^{(T \times f_{FC_{M-1}})}$, where T denotes the number of macromolecular targets in the dataset. The multitask loss function would be, in the case of a classifier:

$$\begin{aligned}
Loss_{multitask} &= \frac{1}{T} \sum_j^T Loss_j \\
&= \frac{1}{T} \sum_j^T \left[\frac{1}{n_j} \sum_i^{n_j} (y_i \cdot \log(\sigma(\hat{y}_i)) + (1 - y_i) \cdot \log(1 - \sigma(\hat{y}_i))) \right],
\end{aligned} \tag{10}$$

which is the average binary cross-entropy loss across the T tasks (targets).

B. Structure-based scoring models

The program of drug discovery since the advent of biomolecular crystallography by Perutz et al.¹⁷ has widened in scope to encompass structural information about the target of interest in addition to information about ligands themselves. Both X-ray crystal structures and, more recently, cryo-EM structures have inspired aspirations for “rational” drug discovery, in which medicinal chemists deduce modifications to scaffolds designed specifically to leverage features of protein or nucleic acid binding domains.

Numerous physics-based approaches have striven to re-

alize this paradigm, including molecular docking^{18–21}, free energy perturbation²², QM/MM²³, among others. More recently, informatic approaches have also taken up the problem of predicting affinity based on dual ligand and structural information, including SPLIF²⁴, RF-Score^{25,26}, NN-score²⁷, Grid Featurizer¹¹, three dimensional convolutional neural network approaches^{28,29}, and Atomic Convolutional Neural Networks^{30,31}. Both NN-Score and Grid Featurizer use the neural network update in (1) in which the feature vector x for each ligand is a flat vector of hand-crafted descriptors of the ligand and of the ligand-protein interaction. For example, Grid Featurizer includes ECFP-4 ligand features, counts of hydrogen bonds and salt bridges, and SPLIF-like fingerprints concatenated together and subsequently provided as input to an FCNN.

1. Spatial Graph Convolutions: Fixed Edge Types

To motivate architectures for more principled deep neural network predictors, we invoke the following notation and framework. First, we introduce the distance matrix $R \in \mathbb{R}^{(N \times N)}$, whose entries R_{ij} denote the distance between $atom_i$ and $atom_j$.

$$R = \begin{bmatrix} R_{11} & R_{12} & \cdots & R_{1N} \\ R_{21} & R_{22} & \cdots & R_{2N} \\ \vdots & \vdots & \ddots & \vdots \\ R_{N1} & R_{N2} & \cdots & R_{NN} \end{bmatrix} \in \mathbb{R}^{N \times N}, \quad (11)$$

where: $R_{ij} = \text{dist}(atom_i, atom_j)$.

Thus far, the concept of adjacency, as encoded in the

$$A = \left(\begin{bmatrix} A_{111} & A_{121} & \cdots & A_{1N1} \\ A_{211} & A_{221} & \cdots & A_{2N1} \\ \vdots & \vdots & \ddots & \vdots \\ A_{N11} & A_{N21} & \cdots & A_{NN1} \end{bmatrix}, \dots, \begin{bmatrix} A_{11N_{\text{et}}} & A_{12N_{\text{et}}} & \cdots & A_{1NN_{\text{et}}} \\ A_{21N_{\text{et}}} & A_{22N_{\text{et}}} & \cdots & A_{2NN_{\text{et}}} \\ \vdots & \vdots & \ddots & \vdots \\ A_{N1N_{\text{et}}} & A_{N2N_{\text{et}}} & \cdots & A_{NNN_{\text{et}}} \end{bmatrix} \right) \quad (12)$$

$$\in \mathbb{R}^{N \times N \times N_{\text{et}}}, \text{ where: } A_{ijk} = \begin{cases} 1, v_j \in N(v_i) \text{ and } e_{i,j} = k \\ 0, \text{ otherwise.} \end{cases}$$

If we order the rows by the membership of $atom_i$ to either the protein or ligand, we can view both A and R as block matrices, where the diagonal blocks are self-edges (i.e., bonds and non-covalent interactions) from one ligand atom to another ligand atom or from one protein atom to another protein atom, whereas off-diagonal block matrices encode edges from the protein to the ligand and from ligand to protein. For illustration purposes, we choose the special case where there is only one edge type, $N_{\text{et}} = 1$:

$$A = \begin{bmatrix} A_{11} & A_{12} & \cdots & A_{1N} \\ A_{21} & A_{22} & \cdots & A_{2N} \\ \vdots & \vdots & \ddots & \vdots \\ A_{N1} & A_{N2} & \cdots & A_{NN} \end{bmatrix} \in \mathbb{R}^{N \times N} \quad (13)$$

$$= \begin{bmatrix} A_{L:L} & A_{L:P} \\ A_{P:L} & A_{P:P} \end{bmatrix},$$

$$\text{where: } A_{ij} = \begin{cases} 1, v_j \in N(v_i) \\ 0, \text{ otherwise.} \end{cases}$$

Within this framework, we can mathematically express a **spatial graph convolution** – a graph convolution

symmetric matrix A (2), has been restricted to chemical bonds, which in turn can be viewed in network parlance as undirected edges. However, one can define adjacency to encompass a wider range of neighbor types. In the setting of biomolecular interactions, in addition to bonds, adjacency could specify noncovalent interactions (e.g., $\pi - \pi$ stacking, hydrogen bonds, hydrophobic contact) as well. An alternative to such domain expertise-driven edge types would be to incorporate notions of distance, either with a real-numbered value or with multiple one-hot distance bins. Regardless of particular edge definition scheme, we see how the distance matrix R can motivate the construction of an expanded version of A . In this framework, A becomes a tensor of shape $N \times N \times N_{\text{et}}$, where N_{et} is an integer representing the number of edge types:

based on notions of adjacency predicated on Euclidean distance relationships – as a generalization of the GGNN given in (8). In particular, in this work we examine two specific realizations of the spatial graph convolution: the Staged Spatial Graph Convolution and the PotentialNet Spatial Graph Convolution.

The staged spatial graph convolution consists of three main steps: (1) covalent-only propagation, (2) dual non-covalent and covalent propagation, and (3) ligand-based graph gather. Stage (1), covalent propagation, entails only the first slice of the adjacency matrix, $A^{(1)}$, which contains a 1 at entry (i, j) if there is a bond between $(atom_i, atom_j)$ and a 0 otherwise. Intuitively, stage (1) computes a new set of vector-valued atom types for each of the N atoms in the system based on their local networks of bonded atoms. Subsequently, stage (2) entails propagation based on both the full adjacency tensor A which begins with the vector-valued atom types computed in (1). While stage (1) computes new bond-based atom types for both amino acid and ligand atoms, stage (2) passes both bond and spatial information between the atoms. For instance, if stage (1) distinguishes an amide carbonyl oxygen from a ketone carbonyl oxygen, stage (2) might communicate in the first layer that that carbonyl oxygen is also within 3 Angstroms of a hydrogen bond donor. Finally, in stage (3) a graph gather is performed solely on the ligand atoms. The ligand-only graph gather is made computationally

straightforward by the block matrix formulation described in (13).

Spatial GGNN, Stage 1:

$$\begin{aligned}
 h^{(bond_1)} &= GRU^{(bond)} \left(x, \sum_e^{N_{bondtypes}} W^{(e)} A^{(e)} x \right) \\
 h^{(bond_2)} &= GRU^{(bond)} \left(h^{(bond_1)}, \sum_e^{N_{bondtypes}} W^{(e)} A^{(e)} h^{(bond_1)} \right) \\
 &\vdots \\
 h^{(bond_K)} &= GRU^{(bond)} \left(h^{(bond_{K-1})}, \sum_e^{N_{bondtypes}} W^{(e)} A^{(e)} h^{(bond_{K-1})} \right) \\
 h^{(bond)} &= \sigma \left(i^{(bond)}(h^{(bond_K)}, x) \right) \odot \left(j^{(bond)}(h^{(bond_K)}) \right) \\
 &\in \mathbb{R}^{(N \times f_{bond})}
 \end{aligned} \tag{14}$$

Spatial GGNN, Stage 2:

$$\begin{aligned}
 h^{(spatial_1)} &= GRU^{(spatial)} \left(h^{(bond)}, \sum_e^{N_{et}} W^{(e)} A^{(e)} h^{(bond)} \right) \\
 h^{(spatial_2)} &= GRU^{(spatial)} \left(h^{(spatial_1)}, \sum_e^{N_{et}} W^{(e)} A^{(e)} h^{(spatial_1)} \right) \\
 &\vdots \\
 h^{(K_{spatial})} &= GRU^{(spatial)} \left(h^{(spatial_{K-1})}, \sum_e^{N_{et}} W^{(e)} A^{(e)} h^{(K-1)} \right) \\
 h^{(spatial)} &= \sigma \left(i^{(spatial)}(h^{(spatial)}, x) \right) \odot \left(j^{(spatial)}(h^{(spatial)}) \right) \\
 &\in \mathbb{R}^{(N \times f_{spatial})}
 \end{aligned} \tag{15}$$

Spatial GGNN, Stage 3:

$$\begin{aligned}
 h^{(FC_0)} &= \sum_{j=1}^{N_{Lig}} h_j^{(spatial)} \\
 h^{(FC_1)} &= ReLU \left(W^{(FC_1)} h^{(FC_0)} \right) \\
 &\vdots \\
 h^{(FC_K)} &= W^{(FC_K)} h^{(FC_{K-1})},
 \end{aligned} \tag{16}$$

where $i^{(bond)}$, $j^{(bond)}$, $i^{(spatial)}$, $j^{(spatial)}$ are neural networks, and $h_j^{(spatial)}$ denotes the feature map for the j^{th} atom at the end of stage 2.

A theoretically attractive concept in (14) is that atom types – the $1 \times f_{bond}$ per-atom feature maps – are derived from the same initial features for both ligand and protein atoms. In contrast to molecular dynamics force

fields (e.g., 32–34), which have distinct force fields for ligands and for proteins which then must interoperate (often poorly) in simulation, we take the approach in this work of deriving the physicochemical properties of biomolecular properties from a unified framework. There is little principled basis for drawing an artificial distinction between the atoms in proteins and the atoms in small organic molecules; a phenolic hydroxyl oxygen is a

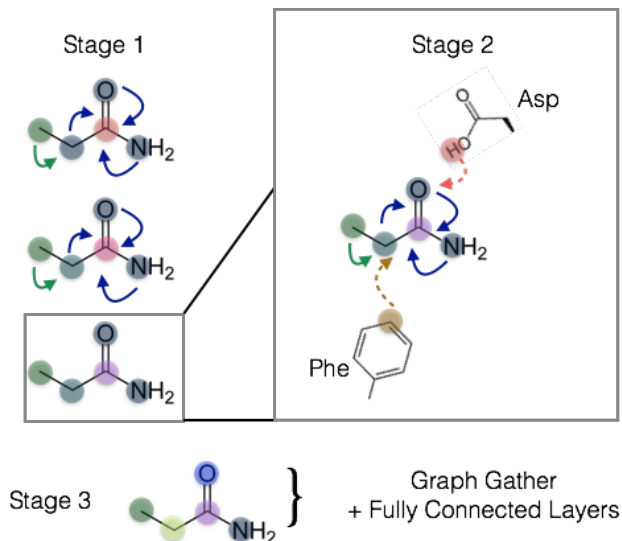


FIG. 2. Visual depiction of multi-staged spatial gated graph neural network. Stage 1 entails graph convolutions over only bonds, which derives new node (atom) feature maps roughly analogous to differentiable atom types in more traditional forms of molecular modeling. While it is not depicted, bond-based propagation is conducted for both ligand and protein atoms. Stage 2 entails both bond-based and spatial distance based propagation of information. In the final stage, a graph gather operation is conducted over the ligand atoms, whose feature maps are derived from bonded ligand information and spatial proximity to protein atoms.

phenolic hydroxyl oxygen whether it is found on tyrosine or on morphine.

2. Spatial Graph Convolutions: Variable Edge Types

It is noteworthy that the staged spatial GGNN described above, like the graph convolutional updates used in 5 and 6, has the same update function $W^{(e)}A^{(e)}$ for

query $atom_i$ regardless of the identity of the source $atom_j$ from which that edge emanates. While from a machine learning perspective one might suspect that this yields better performance by reducing the number of parameters and therefore the variance of resulting models, physical intuition alone might suggest a different approach. The enthalpic contributions to protein-ligand binding free energy stem largely from electrical interactions; hydrogen bonds, aromatic stacking, salt bridges, induced dipoles, and even van der Waals interactions are all categorizations of solutions of Schrodinger’s equation with electric potentials. All of these specific realizations of electric potential energy, from hydrogen bonds to π stacking, can be broken down into components of a source charge distribution, an interacting charge or charge distribution, and the distribution of pairwise distances between them. Therefore, on paper it seems overly reductive to consider the update (focusing on $atom_i$): $h_i^{(K_{spatial})} = GRU^{(spatial)}\left(h_i^{(spatial_{K-1})}, \sum_e^{N_{et}} W^{(e)} A^{(e)} h^{(K-1)}\right)$. A typical deep learning-oriented approach would favor empiricism over domain expertise and delineate the N_{et} edge types as dependent only on the distance matrix R ; therefore, the message for $atom_i$ at layer K would be the i ’th row vector of $\sum_e^{N_{et}} W^{(e)} A^{(e)} h^{(K-1)}$. Since the weight matrices $W^{(e)}$ depend solely on the distance-based edge type e and not on the sources $h^{(K-1)}$ of those edges, we arrive at the counterintuitive regime where qualitatively different nodes are acted upon by the same linear functions to determine their contribution to the message.

For example, a negatively charged carboxylic acid oxygen that is 3 Angstroms away from some query $atom_i$ will be acted upon by the same weight matrices as a positively charged arginine nitrogen that is 3 Angstroms away from the same query $atom_i$. It therefore makes sense from a standpoint of physicochemical intuition to render the message emanating from a given $atom_j$ depend on both its distance and its distinct properties. Such a proposal can be expressed as follows:

PotentialNet

$$\begin{aligned}
 h_i^{(1)} &= GRU \left(x_i, \sum_{v_j \in N(v_i)} NN(e_{ij}, x_j) \right) \\
 h_i^{(2)} &= GRU \left(h_i^{(1)}, \sum_{v_j \in N(v_i)} NN(e_{ij}, h_j^{(1)}) \right) \\
 &\vdots \\
 h_i^{(K)} &= GRU \left(h_i^{(K-1)}, \sum_{v_j \in N(v_i)} NN(e_{ij}, h_j^{(K-1)}) \right) \\
 h_i^{(spatial)} &= \sigma \left(i^{(spatial)}(h^{(K)}, x) \right) \odot \left(j^{(spatial)}(h^{(K)}) \right) \\
 h^{(FC_0)} &= \sum_{j=1}^{N_{Lig}} h_j^{(spatial)} \\
 &\in \mathbb{R}^{(1 \times f_{gather})} \\
 h^{(FC_1)} &= ReLU \left(W^{(FC_1)} h^{(FC_0)} \right) \\
 &\vdots \\
 h^{(FC_K)} &= W^{(FC_K)} h^{(FC_{K-1})},
 \end{aligned} \tag{17}$$

where i , j , and NN are neural networks. Since the update operation $GRU \left(h_i^{(K-1)}, \sum_{v_j \in N(v_i)} NN(e_{ij}, h_j^{(K-1)}) \right)$ is a function that incorporates the origin atoms and the atoms to which they are connected via the message operation, intuitively we contend that there is no need to include both the source node $atom_i$ and terminus node $atom_j$ in the message operation $NN(e_{ij}, h_j^{(1)})$; a more complex update function $NN(e_{ij}, h_j^{(1)}, h_i^{(1)})$ might therefore be redundant with the GRU operation. For this reason, we denote this architecture as a PotentialNet. Just as the electrostatic potential is computed as $\phi = \sum \frac{1}{4\pi\epsilon_0} \frac{q_i}{|\vec{r}_i - \vec{r}|}$, dependent on both the distance from and the charge of source charges (nodes), network (17) computes in the message function an analogue to a “field” dependent on both the distances and feature maps of a set of neighbor nodes.

III. MEASURING EARLY ENRICHMENT IN REGRESSION SETTINGS FOR VIRTUAL SCREENING

Traditional metrics of performance of predictors suffer from both general problems and from issues specific to the drug discovery process. For regressors, both R^2 —the “coefficient of determination”—and the root-mean-square error ($RMSE$) are susceptible to single data point outliers. The $RMSE$ for both classifiers and regressors account neither for the distribution of the training data nor the

performance of a null model. While the area under the receiver operating characteristic curve (AUC)³⁵ corrects for this deficiency in $RMSE$ for classifiers, it suffers from the same intrinsic issue common to all aforementioned metrics: they are global statistics that equally weight all data points. Such a property may be desired in many settings. However, in a drug discovery setting, one is generally interested in performance at predicting the tails of a distribution. A virtual screening library might contain millions of molecules; while one will make model predictions against all such compounds, one will likely only purchase or synthesize a small fraction comprising the top scoring molecules in that library.

When, for all practical purposes, one can only take actions based on the tails of the distribution, it makes intuitive sense to measure model performance on those tails. As a result, the concept of **early enrichment** has risen in currency in the cheminformatics community. Methods like $BEDROC$ ³⁶ and $LogAUC$ ³⁷ weight the importance of the highest performers according to the model more heavily than lower performers. In other words, those molecules which the model predicts are the most active will affect $BEDROC$ or $LogAUC$ more than molecules which the model predicts are mediocre or poor binders. While $BEDROC$ and $LogAUC$ are, like AUC , bounded between 0.0 and 1.0, the enrichment factor (EF_χ)³⁸ measures the proportion of actives in the top $\chi\%$ scoring compounds divided by the proportion of actives in the overall population.

A. Proposed Metric: $EF_{\chi}^{(R)}$

At present, this progress in early enrichment measurement has been limited to classification and has yet to include regression. Therefore, we propose a new metric, $EF_{\chi}^{(R)}$, analogous to EF_{χ} , which measures early enrichment in regression. For a given target:

$$EF_{\chi}^{(R)} = \frac{1}{\chi \cdot N} \sum_i^{\chi \cdot N} \frac{y_i - \bar{y}}{\sigma(y)} \quad (18)$$

$$= \frac{1}{\chi \cdot N} \sum_i^{\chi \cdot N} z_i, \quad (19)$$

in which y_i , the experimental (observed) measurement for sample i , are ranked in descending order according to \hat{y}_i , the model (predicted) measurement for sample i . In other words, for the top $\chi\%$ scoring samples, we compute the average z-score—average number of standard deviations away from the mean—for the observed values of those top $\chi\%$ scoring compounds. We prefer this approach to computing, for example, $\frac{1}{\chi \cdot N} \sum_i^{\chi \cdot N} (y_i - \bar{y})$, which has units that are the same as y_i (i.e., $\log(K_i)$ values). However, the latter, unnormalized approach has the disadvantage of dependence on the distribution in the dataset. For instance, in a distribution of $\log(K_i)$ measurements, if the maximum deviation from the mean is 1.0, the best a model can possibly perform would be to achieve an $EF_{\chi}^{(R)}$ of 1.0. Normalizing through division by $\sigma(y)$, the standard deviation of the dataset, renders model performance comparable amongst different datasets with a common unit of measurement but perhaps different variances in those measurements.

A common approach in measuring virtual screening performance is to measure per-target performance. Another deficiency in metrics like AUC or $RMSE$ is that they treat all compounds as equally weighted even if one is measuring/predicting their affinity at different target biological macromolecules. We therefore propose, when reporting results on datasets of significant size, to compute the $EF_{\chi}^{(R)}$ on individual targets, and either take the mean or median of the result,

$$EF_{\chi}^{(R)} = \frac{1}{T} \sum_j^T \left(\frac{1}{\chi \cdot N_j} \sum_i^{\chi \cdot N_j} \frac{y_i^{(j)} - \bar{y}^{(j)}}{\sigma(y^{(j)})} \right) \quad (20)$$

$$= \frac{1}{T} \sum_j^T \left(\frac{1}{\chi \cdot N_j} \sum_i^{\chi \cdot N_j} z_i^{(j)} \right), \quad (21)$$

where T is the total number of target molecules, N_j is the number of samples predicted for target j , and $\bar{y}^{(j)}$ is the mean of experimental measurements for target j .

IV. RESULTS

A. Cross-validation strategies

It is well known that the performance of deep neural network algorithms is highly sensitive to chosen hyperparameters. Such sensitivity underscores the criticality of rigorous cross-validation^{39,40}. Several recent papers, including works that claim specifically to improve binding affinity prediction on the PDBBind dataset^{41,42}, engage in the practice of *searching hyperparameters directly on the test set*. Compounding this problem is a fundamental deficiency of the main cross-validation procedure used in this subfield that is discussed below.

While there are newer iterations of the PDBBind dataset^{43–45}, in order to compare performance of our proposed architectures to previous methods we choose to evaluate performance based on PDBBind 2007^{46,47}. In previous works, the PDBBind 2007 dataset was split by (1) beginning with the “refined” set comprising 1,300 protein-ligand co-crystal structures and associated binding free energy values; (2) removing the “core” set comprising 195 samples to form the test set, with (3) the remaining 1,095 samples serving as the training data. We term this train-test split “PDBBind 2007, Refined Train, Core Test”, below, and compare performance with RF-score²⁶, X-Score^{48,49}, and the networks (14)-(16) and (17) described in this work.

Although employing the same dataset and train-test split as previous methods enables the direct comparison that serves as the foundation for the advancement of statistical learning, it also entails intrinsic drawbacks; namely, while no gradient information stems from the test set during training, it is still possible to overfit to the test set through hyperparameter searching. Another drawback to this cross-validation strategy is that the train and test sets will contain many similar examples, whether in terms of structural or sequence homology between train and test proteins or chemical composition similarity between train and test ligands. Whereas it is typical in other machine learning disciplines for the train and test set examples to be drawn from the same statistical distributions, such a setting is not necessarily desirable in a molecular machine learning setting⁵⁰. Drug discovery campaigns typically involve the synthesis and investigation of novel chemical matter. In order to accurately assess the capacity of a trained model to generalize in its predictive ability of the chemical properties of new matter, one must pursue a cross-validation strategy that reflects how that model will be deployed practically.

In context of this reasoning, it is arguable that the “Refined Train, Core Test” strategy is not an optimal choice of cross-validation strategy. First, there are several proteins in the core (test) set that are also included with in the train set (though with different PDB IDs and different co-crystallized ligands). Even if the proteins are not identical, there are core set proteins for which there are highly homologous—by measure of sequence or struc-

ture⁵¹—proteins in the train set. Compounding the issue of similar (or identical) proteins, similar proteins tend to bind to similar ligands, at least in PDBBind 2007⁵¹. In 51, it was shown that systematically removing samples from the PDBBind 2007 refined set with structural or sequence homology to the core (test) set significantly attenuated the performance of recent ML-based methods for affinity prediction. Therefore, we suggest a cross-validation strategy that splits all of the training data into three distinct folds—train, validation, and test subsets—according to the similarity of the molecular representation^{51,52}.

B. Performance of methods on benchmarks

On the standard PDBBind 2007 “refined train, core test” benchmark, Spatial Graph Convolutions achieve state-of-the-art performance as reflected by several metrics. Both the standard Spatial Graph Convolution (14)-(16) and the PotentialNet Spatial Graph Convolution (17) outperform RF-Score and X-Score according to Pearson and Spearman correlation coefficients. The Pearson correlation score for standard Spatial Graph Convolution (14)-(16) is within error of the reported score for TopologyNet, the heretofore top performing model on this benchmark. However, a key caveat must be noted with respect to this comparison. As described in the Methods section of this work, all cross-validation for this manuscript, including all of our results reported in Table I, was performed such that performance on the *test* set was recorded for the hyperparameter set that performed most highly on the distinct *validation* set. In contrast, the TopologyNet paper⁴¹, models were trained on a *combination* of the validation and training sets and evaluated *directly on the test set*. Performance for TopologyNet⁴¹ therefore reflects a train-validation type split rather than a train-validation-test split, which likely inflated the performance of that method. The direct comparison in Table 1 between TopologyNet and other methods should therefore be viewed with this caveat in mind.

It is noteworthy that Spatial Graph Convolutions of all reported varieties [(14)-(16) and (17)] perform competitively with other compared methods when the proposed Spatial Graph Convolutions are predicated on very simple, per-atom features and pure notions of distance whereas RF-Score, X-Score, and TopologyNet all directly incorporate domain-expertise driven information on protein-ligand interactions.

V. DISCUSSION

A key discrepancy separates machine learning for molecular sciences from other domains: the largest publicly available dataset of high quality protein-ligand binding affinities and their associated co-crystal structures is PDBBind 2016⁴⁵ with 4,057 samples, whereas ImageNet⁵³ currently contains over 14,000,000 labeled images. Faced

with such a comparative paucity of data, molecular scientists have had particular motivation to conceive of innovative models in order to maximize the performance of their affinity prediction models. We contribute to this expanding literature by proposing a family of new neural network architectures for affinity prediction. We demonstrate how these models stem from the common framework of the Spatial Graph Convolution.

The Spatial Graph Convolutions exhibit state-of-the-art performance in context of its recent predecessors. On the traditional PDBBind 2007 benchmark, where 1,105 samples from the refined set serve as training data and 195 samples from the core set serve as test data, Spatial Graph Convolutions exceed the performance of X-Score and RF-Score while showing comparable performance with TopologyNet (with the key caveat that the latter paper searched hyperparameters directly over the test dataset). That said, we suggest that practitioners consider the practical utility of their cross-validation splitting algorithm. As a field with immense practical applications, we need to design our algorithms with realizable results in mind, and not seek incrementally higher numbers on perhaps arbitrary benchmarks. For this reason, we have presented a cross-validation procedure in order to motivate other groups to design algorithms that are more likely to directly aid drug discovery efforts.

In context of both this competitive performance, the benefits and potential drawbacks of our models should be discussed. In contrast to RF-score, X-score, TopologyNet, and similar methods in this family, which take traditional physics-based features and incorporate those features into machine learning models, the Spatial Graph Convolutions described in this work take a more principled deep learning approach: input features are restricted to basic information about atoms, bonds, and distances, and higher-level interaction “features” are learned in intermediate graph convolutional neural network layers that enable fully connected layers to estimate energy. Without preconceived definitions of such terms as hydrophobic effects, solvation, hydrogen bonding, aromatic interactions, etc., Spatial Graph Convolutions based on basic features can learn complex and accurate relationships that map input protein-ligand structures to binding free energies. Since this more complex mapping is learned on the same, relatively low amount of data as previous domain expertise-driven approaches, we expect that Spatial Graph Convolutions will have the capacity to become the gold standard in affinity prediction if applied in a setting where more sizable collections of training data become available. Alas, since larger publicly available datasets of protein-ligand structures and their associated binding affinities are, at present, nonexistent, we call upon a consortium of academic experimental scientists and/or their pharmaceutical industry counterparts to release as much high quality protein-ligand binding affinity data as possible so the field as a whole can progress in developing generalizable affinity models to all parties’ mutual benefit.

TABLE I. Benchmark: PDBBind 2007, Refined Train, Core Test

Model	Test R^2	Test $EF_{\chi}^{(R)}$	Test Pearson	Test Spearman	Test stdev	Test MUE
Spatial MPNN	0.668 (0.043)	1.643 (0.127)	0.822 (0.021)	0.826 (0.020)	1.388 (0.070)	0.626 (0.037)
Spatial MPNN PotentialNet	0.607 (0.062)	1.724 (0.263)	0.795 (0.040)	0.785 (0.035)	1.473 (0.114)	0.692 (0.050)
MPNN, Ligand-only	0.419 (0.234)	1.404 (0.171)	0.650 (0.017)	0.670 (0.014)	1.832 (0.135)	0.839 (0.005)
TopologyNet ⁴¹ , No Validation Set	N/A	N/A	0.826	N/A	N/A	N/A
RF-Score ⁵¹	N/A	N/A	0.783	0.769	N/A	N/A
X-Score ⁵¹	N/A	N/A	0.643	0.707	N/A	N/A

METHODS

Deep neural networks were constructed and trained with PyTorch⁵⁴. Featurization was conducted with custom Python code based on RDKit⁸ and OEChem⁹, with frequent use of the SciPy Sparse package⁵⁵ and NumPy⁵⁶. RF-score and X-score models were trained with the Random Forest and linear regression implementations, respectively, in the scikit-learn package⁵⁷.

Cross-validation on PDBBind 2007 core test set benchmark was performed with the following procedure. First, the core set was removed from the refined set to construct the train set. The resulting train set was sorted temporally. Then, up to eight hyperparameters were designated for tuning. Since this spanned thousands of possible hyperparameter combinations, grid search would be inefficient and therefore random hyperparameter search was used instead. For each randomly generated hyperparameter set, K-fold temporal cross validation within the train set was conducted. For each of the K held-out folds (where each fold served as a validation set), validation set performance was recorded at that epoch at which Pearson correlation coefficient between the labeled and predicted values in the validation set was highest. The validation score for each hyperparameter set was recorded as the average Pearson score over the K-folds at the best epoch for each fold. The hyperparameter set with the best average Pearson score was used to evaluate test set performance. The training set was split into K temporal folds, and for each of the folds, test set performance was recorded at the epoch at which the validation set performance was highest according to Pearson score. Reported metrics—Pearson coefficient, Spearman coefficient, mean unsigned error (MUE), Regression Enrichment Regression, and r^2 —are each reported as the median score with the standard deviation over the K folds in parentheses.

ACKNOWLEDGMENTS

V.S.P. is a consultant & SAB member of Schrodinger, LLC and Globavir, sits on the Board of Directors of Apeel Inc, Freenome Inc, Omada Health, Patient Ping, Rigetti Computing, and is a General Partner at Andreessen Horowitz. E.N.F. is supported by the Blue Waters Graduate Fellowship. We acknowledge the generous support of Dr. Anders G. Frøseth and Mr. Christian Sundt for our work on machine learning. The Pande Group is broadly supported by grants from the NIH (R01 GM062868 and U19 AI109662) as well as gift funds and contributions from Folding@home donors. B.R. was supported by the Fannie and John Hertz Foundation.

AUTHOR CONTRIBUTIONS

E.N.F. conceived and designed the neural network architectures. E.N.F. and D.S. implemented the neural networks. B.E.H. implemented cross-validation. D.M, Y.L., and J.Y. contributed critical datasets and trained random forests-based and linear regression-based models. E.N.F. and B.E.H. wrote the manuscript. E.N.F., B.R., and V.S.P. supervised the project.

¹R. Bellman, "Adaptative control processes," (1961).

²T. Hastie, R. Tibshirani, and J. Friedman, in *The Elements of Statistical Learning* (Springer, 2009) pp. 9–41.

³S. Kearnes, K. McCloskey, M. Berndl, V. Pande, and P. Riley, *J. Comput. Aided Mol. Des.* **30**, 595 (2016).

⁴T. N. Kipf and M. Welling, arXiv preprint arXiv:1609.02907 (2016).

⁵Y. Li, D. Tarlow, M. Brockschmidt, and R. Zemel, arXiv preprint arXiv:1511.05493 (2015).

⁶J. Gilmer, S. S. Schoenholz, P. F. Riley, O. Vinyals, and G. E. Dahl, arXiv preprint arXiv:1704.01212 (2017).

⁷V. Nair and G. E. Hinton, in *Proceedings of the 27th International Conference on Machine Learning (ICML-10)* (2010) pp. 807–814.

⁸RDKit: Open-source cheminformatics; <http://www.rdkit.org>.

⁹OEChem OpenEye Scientific Software, Santa Fe, NM. <http://www.eyesopen.com>.

TABLE II. Hyperparameters for neural network (14)-(16)

Hyperparameter Name	Symbol	Possible Values
Bond Gather Width	f_{bond}	[64, 128]
Spatial Gather Width	$f_{spatial}$	[64, 128]
Fully Connected Widths	n_{rows} of $W^{(FC_i)}$	[[128, 32, 1], [128, 1], [64, 32, 1], [64, 1]]
Number of Bond Convolution Layers	$bond_K$	[1, 2]
Number of Spatial Convolution Layers	$spatial_K$	[1, 2, 3]
Learning Rate	-	[1e-3, 2e-4]
Weight Decay	-	[0., 1e-7, 1e-5, 1e-3]
Dropout	-	[0., 0.25, 0.4, 0.5]

TABLE III. Hyperparameters for neural network (17)

Hyperparameter Name	Symbol	Possible Values
Gather Width	f_{gather}	[64, 128]
Fully Connected Widths	n_{rows} of $W^{(FC_i)}$	[[128, 32, 1], [128, 1], [64, 32, 1], [64, 1]]
Number of Graph Convolution Layers	K	[1, 2, 3]
Learning Rate	-	[1e-3, 2e-4]
Weight Decay	-	[0., 1e-7, 1e-5, 1e-3]
Dropout	-	[0., 0.25, 0.4, 0.5]

- ¹⁰N. M. O’Boyle, M. Banck, C. A. James, C. Morley, T. Vandermeersch, and G. R. Hutchison, *Journal of cheminformatics* **3**, 33 (2011).
- ¹¹Z. Wu, B. Ramsundar, E. N. Feinberg, J. Gomes, C. Geniesse, A. S. Pappu, K. Leswing, and V. Pande, arXiv preprint arXiv:1703.00564 (2017).
- ¹²D. Rogers and M. Hahn, *J. Chem. Inf. Model.* **50**, 742 (2010).
- ¹³P. C. Hawkins, A. G. Skillman, and A. Nicholls, *J. Med. Chem.* **50**, 74 (2007).
- ¹⁴S. Kearnes and V. Pande, *J. Comput. Aided Mol. Des.* **30**, 609 (2016).
- ¹⁵A. Krizhevsky, I. Sutskever, and G. E. Hinton, in *Advances in Neural Information Processing Systems* (2012) pp. 1097–1105.
- ¹⁶D. K. Duvenaud, D. Maclaurin, J. Iparraguirre, R. Bombarell, T. Hirzel, A. Aspuru-Guzik, and R. P. Adams, in *Advances in Neural Information Processing Systems* (2015) pp. 2224–2232.
- ¹⁷M. F. Perutz, M. G. Rossmann, A. F. Cullis, H. Muirhead, G. Will, and A. North, *Nature* **185**, 416 (1960).
- ¹⁸A. N. Jain, *J. Med. Chem.* **46**, 499 (2003).
- ¹⁹B. K. Shoichet, I. D. Kuntz, and D. L. Bodian, *J. Comput. Chem.* **13**, 380 (1992).
- ²⁰O. Trott and A. J. Olson, *J. Comput. Chem.* **31**, 455 (2010).
- ²¹R. A. Friesner, J. L. Banks, R. B. Murphy, T. A. Halgren, J. J. Klicic, D. T. Mainz, M. P. Repasky, E. H. Knoll, M. Shelley, J. K. Perry, *et al.*, *J. Med. Chem.* **47**, 1739 (2004).
- ²²L. Wang, Y. Wu, Y. Deng, B. Kim, L. Pierce, G. Krilov, D. Lupyan, S. Robinson, M. K. Dahlgren, J. Greenwood, *et al.*, *J. Am. Chem. Soc.* **137**, 2695 (2015).
- ²³C. Hensen, J. C. Hermann, K. Nam, S. Ma, J. Gao, and H.-D. Höltje, *J. Med. Chem.* **47**, 6673 (2004).
- ²⁴C. Da and D. Kireev, *J. Chem. Inf. Model.* **54**, 2555 (2014).
- ²⁵H. Li, K.-S. Leung, M.-H. Wong, and P. J. Ballester, *Mol. Inform.* **34**, 115 (2015).
- ²⁶P. J. Ballester and J. B. Mitchell, *Bioinformatics* **26**, 1169 (2010).
- ²⁷J. D. Durrant and J. A. McCammon, *J. Chem. Inf. Model.* **51**, 2897 (2011).
- ²⁸I. Wallach, M. Dzamba, and A. Heifets, arXiv preprint arXiv:1510.02855 (2015).
- ²⁹M. Ragoza, J. Hochuli, E. Idrobo, J. Sunseri, and D. R. Koes, *J. Chem. Inf. Model.* **57**, 942 (2017).
- ³⁰J. Gomes, B. Ramsundar, E. N. Feinberg, and V. S. Pande, arXiv preprint arXiv:1703.10603 (2017).
- ³¹M. Ragoza, L. Turner, and D. R. Koes, arXiv preprint arXiv:1710.07400 (2017).
- ³²J. W. Ponder and D. A. Case, *Adv. Protein Chem.* **66**, 27 (2003).
- ³³D. A. Case, T. E. Cheatham, T. Darden, H. Gohlke, R. Luo, K. M. Merz, A. Onufriev, C. Simmerling, B. Wang, and R. J. Woods, *J. Comput. Chem.* **26**, 1668 (2005).
- ³⁴B. R. Brooks, C. L. Brooks, A. D. MacKerell, L. Nilsson, R. J. Petrella, B. Roux, Y. Won, G. Archontis, C. Bartels, S. Boresch, *et al.*, *J. Comput. Chem.* **30**, 1545 (2009).
- ³⁵N. Triballeau, F. Acher, I. Brabet, J.-P. Pin, and H.-O. Bertrand, *J. Med. Chem.* **48**, 2534 (2005).
- ³⁶J.-F. Truchon and C. I. Bayly, *J. Chem. Inf. Model.* **47**, 488 (2007).
- ³⁷M. M. Mysinger and B. K. Shoichet, *J. Chem. Inf. Model.* **50**, 1561 (2010).
- ³⁸D. A. Pearlman and P. S. Charifson, *J. Med. Chem.* **44**, 502 (2001).
- ³⁹A.-L. Boulesteix, *PLoS Comput. Biol.* **11**, e1004191 (2015).
- ⁴⁰D. Chicco, *BioData Min.* **10**, 35 (2017).
- ⁴¹Z. Cang and G. Wei, *PLoS Comput. Biol.* **13**, e1005690 (2017).
- ⁴²J. Jiménez Luna, M. Skalic, G. Martínez-Rosell, and G. De Fabritiis, *J. Chem. Inf. Model.* (2018).
- ⁴³Y. Li, Z. Liu, J. Li, L. Han, J. Liu, Z. Zhao, and R. Wang, *J. Chem. Inf. Model.* **54**, 1700 (2014).
- ⁴⁴Z. Liu, Y. Li, L. Han, J. Li, J. Liu, Z. Zhao, W. Nie, Y. Liu, and R. Wang, *Bioinformatics* **31**, 405 (2014).
- ⁴⁵Z. Liu, M. Su, L. Han, J. Liu, Q. Yang, Y. Li, and R. Wang, *Acc. Chem. Res.* **50**, 302 (2017).
- ⁴⁶R. Wang, X. Fang, Y. Lu, and S. Wang, *J. Med. Chem.* **47**, 2977 (2004).
- ⁴⁷R. Wang, X. Fang, Y. Lu, C.-Y. Yang, and S. Wang, *J. Med. Chem.* **48**, 4111 (2005).
- ⁴⁸R. Wang, L. Lai, and S. Wang, *J. Comput. Aided Mol. Des.* **16**, 11 (2002).
- ⁴⁹R. Wang, Y. Lu, and S. Wang, *J. Med. Chem.* **46**, 2287 (2003).
- ⁵⁰E. J. Martin, V. R. Polyakov, L. Tian, and R. C. Perez, *J. Chem. Inf. Model.* **57**, 2077 (2017).
- ⁵¹Y. Li and J. Yang, *J. Chem. Inf. Model.* **57**, 1007 (2017).

TABLE IV. Per-node featurization for neural networks trained in this paper

Feature Description	
Element	One-Hot of C, N, O, S, F, Cl, P, etc. (42 total)
Degree	One-Hot of total number of atoms bonded to atom
Number of Hydrogens	One-hot of implicit + explicit hydrogens
Number of Implicit Hydrogens	One-hot of implicit hydrogens
Formal Charge	integer of formal charge
Number of radical electrons	integer of number of radical electrons
Hybridization	one-hot of hybridization type
Aromaticity	Boolean of whether atom is in aromatic ring

⁵²B. E. Husic and V. S. Pande, arXiv preprint arXiv:1712.07704 (2017).

⁵³J. Deng, W. Dong, R. Socher, L.-J. Li, K. Li, and L. Fei-Fei, in *Computer Vision and Pattern Recognition, 2009. CVPR 2009. IEEE Conference on* (IEEE, 2009) pp. 248–255.

⁵⁴A. Paszke, S. Gross, S. Chintala, G. Chanan, E. Yang, Z. DeVito, Z. Lin, A. Desmaison, L. Antiga, and A. Lerer, (2017).

⁵⁵E. Jones, T. Oliphant, P. Peterson, *et al.*, “SciPy: Open source scientific tools for Python,” (2001–).

⁵⁶S. v. d. Walt, S. C. Colbert, and G. Varoquaux, *Computing in Science & Engineering* **13**, 22 (2011).

⁵⁷F. Pedregosa, G. Varoquaux, A. Gramfort, V. Michel, B. Thirion, O. Grisel, M. Blondel, P. Prettenhofer, R. Weiss, V. Dubourg, *et al.*, *J. Mach. Learn. Res.* **12**, 2825 (2011).